ORGANOMETALLICS
Article
Cite This: Organometallics XXXX, XXX, XXX−XXX
pubs.acs.org/Organometallics

Lysosome-Targeted Phosphine-Imine Half-Sandwich Iridium(III) Anticancer Complexes: Synthesis, Characterization, and Biological Activity

Yuliang Yang, Lihua Guo,* Zhenzhen Tian, Xingxing Ge, Yuteng Gong, Hongmei Zheng, Shaopeng Shi, and Zhe Liu*

Institute of Anticancer Agents Development and Theranostic Application, The Key Laboratory of Life-Organic Analysis and Key Laboratory of Pharmaceutical Intermediates and Analysis of Natural Medicine, Department of Chemistry and Chemical Engineering, Qufu Normal University, Qufu 273165, China

Supporting Information

ABSTRACT: The synthesis, characterization, and catalytic ability of converting coenzyme NADH to NAD^+ and the anticancer activity of half-sandwich iridium(III) complexes with general formula of $[(\eta^5\text{-}Cp^x)Ir(P\text{^}N)Cl]PF_6$ (Cp^x: Cp* or biphenyl Cp^{xbiph} derivatives; P^N: various phosphine-imine ligands) were investigated. The crystal structure of the complex **Ir4** showed a piano-stool geometry around the iridium(III) center. This type of iridium(III) complexes had sufficient stability in aqueous solution. Most of the complexes showed good anticancer activities toward A549 cancer cells, which were higher than the clinical drug cisplatin. In this series, complex **Ir8** displayed the highest anticancer activity against A549 cells (IC_{50} = 4.7 μM), showing an approximately 4.5-fold more potent activity than cisplatin (IC_{50} = 21.30 μM). The structure−activity relationship study showed that the cytotoxicity of these complexes may be primarily attributed to the coordination between iridium(III) and the coordinating atoms, and the nature of the imine N-substituents may not be a major factor affecting cytotoxicity. Furthermore, this family of complexes causes cell death by cell stress, inducing apoptosis and necrosis, overproduction of reactive oxygen species, and disruption of the mitochondrial membrane potential. Most interestingly, the use of confocal microscopy provides insights into the microscopic mechanism that the typical complex **Ir3** can penetrate into A549 cancer cells through a non-energy-dependent pathway and specifically distribute in lysosomes.

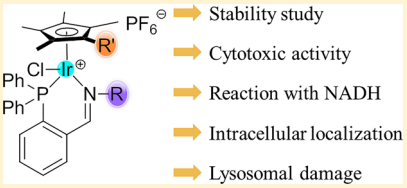

INTRODUCTION

Cancer is one of the leading causes of death worldwide.[1] Platinum-based anticancer drugs are the predecessor of inorganic chemotherapeutic drugs for the treatment of various cancer types.[2−4] However, the side effects of platinum drugs, such as nausea, vomiting, losing hair, drug resistance, and substantial side effects affect fast-growing tissues, thereby limiting their clinical usefulness.[5−9] Thus, researchers focus on discovering non-platinum metallodrugs with reduced side effects and coordination properties.

Anticancer metallodrugs are continuously developed in the field of bioorganometallic chemistry depending upon the rational design of novel and sophisticated ligand frameworks to obtain effective chemotherapeutic agents with a superior toxicity profile. Among these heavy metal complexes, bidentate chelating ligands bearing phosphorus and/or nitrogen donor atoms have wide applications, such as homogeneous catalysts[10−15] and anticancer drugs.[16−23] Modifications of the bidentate chelating ligands of anticancer metallodrugs, such as alteration of the steric and electronic properties of the P- or N-bound substituents, are effective strategies to tune the chemical and biological properties of the compounds. Many organometallic anticancer complexes bearing symmetrical phosphorus or nitrogen donor atoms in their bidentate chelating ligands have been reported.[24−29] For instance, Quirante et al. designed a group of nonplanar cycloplatinated complexes with bidentate phosphine ligand and 2-phenylaniline ligand (Scheme 1, **I**).[24]

Scheme 1. Reported Transition-Metal Anticancer Complexes and Our Current Work

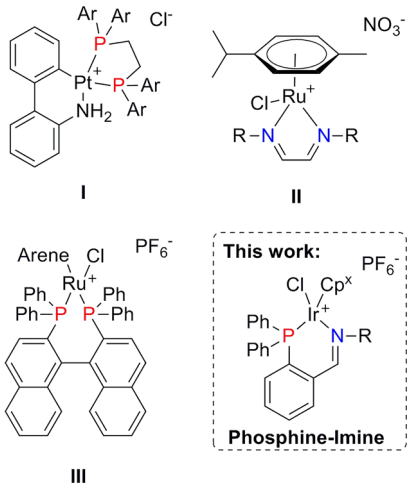

Received: February 6, 2019

DOI: 10.1021/acs.organomet.9b00080
Organometallics XXXX, XXX, XXX−XXX

The high antiproliferative activity of such complexes toward four selected cell lines was attributed to a catalytic process, which produces H_2O_2 as reactive oxygen species (ROS). This oxidant mechanism of action (MoA), which is different from that of platinum drugs, is similar to those of half-sandwich iridium(III) complexes.[30] Additionally, Marchetti's group synthesized a set of water-soluble half-sandwich ruthenium(II) complexes with varying α-diimine ligands (Scheme 1, **II**).[25] The toxicological properties of such complexes depend on the nature of the α-diimine N-substituents. Our group developed a family of half-sandwich iridium(III) and ruthenium(II) complexes bearing P,P-chelated ligands (Scheme 1, **III**).[26] These complexes showed anticancer potency superior to that of cisplatin, and the toxicity properties may be related to the redox MoA. These studies motivated us to synthesize half-sandwich iridium(III) complexes containing phosphine-imine (P^N) chelating ligands and investigate their biological activity.

Herein, we report the synthesis, characterization, and cytotoxic properties against the A549 cancer cell line and the catalytic transfer hydrogenation activity of half-sandwich iridium(III) complexes as supported by various phosphine-imine ligands with a general formula of $[(\eta^5\text{-Cp}^x)\text{Ir(P^N)Cl}]\text{-PF}_6$. To our knowledge, this is the first in vitro evaluation of these novel phosphine-imine half-sandwich iridium(III) complexes for their cytotoxic activity against the A549 cancer cell. The effect of adjusting the coordination environment of the imine moiety on the catalytic ability in converting coenzyme NADH to NAD^+ and anticancer activity was discussed. Moreover, to better understand their MoAs, we investigated the chemical and biological behavior and the cellular imaging property of these complexes.

RESULTS AND DISCUSSION

Synthesis and Characterization. New half-sandwich iridium(III) complexes **Ir1**−**Ir8** were prepared via well-established procedures as illustrated in Scheme 2 and Table 1.

Scheme 2. Synthesis Route of Phosphine-Imine Half-Sandwich Iridium(III) Complexes Ir1−Ir8

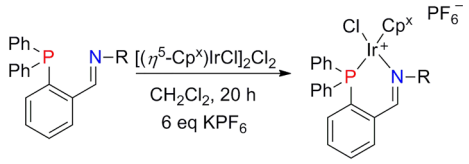

L1-L6 Ir1-Ir8

These complexes were successfully prepared in moderate yields (46−78%) by reacting $[(\eta^5\text{-Cp*})\text{IrCl}_2]_2$ or $[(\eta^5\text{-Cp}^{\text{xbiph}})\text{IrCl}_2]_2$ with corresponding phosphine-imine ligands **L1**−**L6** in a 1:2 molar ratio at room temperature in CH_2Cl_2 (Scheme 2). The complexes **Ir1**−**Ir8** were isolated as their PF_6^- salts and were characterized by multinuclear NMR spectroscopy (Figures S1−S16), Fourier transform infrared (FT-IR) spectroscopy (Figures S17−S24), mass spectrometry (Figures S25−S32), elemental analysis, and X-ray crystallography. The characteristic peaks in the ^{1}H NMR of these complexes were found at δ 8.07−8.79 ppm, which corresponded to the proton of the C(H)═N group. Also, the characteristic peaks of the coordinating phosphorus atom of these complexes were found at δ 6.64−12.32 ppm in the ^{31}P NMR spectra. In addition, the C═N stretching vibrations

Table 1. Organometallic Ir^{III} Cyclopentadienyl $[(\eta^5\text{-Cp}^x)\text{Ir(P^N)Cl}]\text{PF}_6$ Complexes Studied in This Work

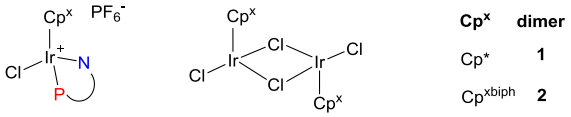

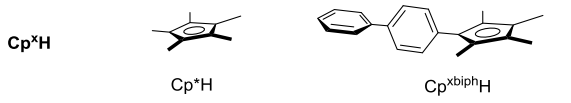

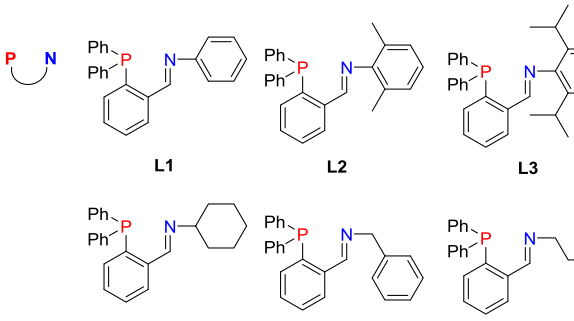

complex	Cp^x	P^N
Ir1	Cp*	**L1**
Ir2	Cp*	**L2**
Ir3	Cp*	**L3**
Ir4	Cp*	**L4**
Ir5	Cp*	**L5**
Ir6	Cp*	**L6**
Ir7	Cp^{xbiph}	**L4**
Ir8	Cp^{xbiph}	**L6**

for complexes **Ir1**−**Ir8** were observed at 1586.9−1617.4 cm^{-1} in the FT-IR spectra.

X-ray Crystal Structures. The molecular structure of complex **Ir4** was confirmed by single-crystal X-ray diffraction. Crystallographic collection and refinement data are summarized in Tables S1 and S2. As illustrated in Figure 1, complex **Ir4** adopts the general pseudo-octahedral three-legged piano-stool configuration, with the phosphine-imine chelating ligand occupying two coordination positions, the pentamethylcyclo-

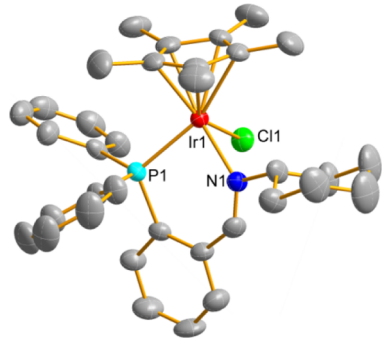

Figure 1. X-ray crystal structure of $[(\eta^5\text{-Cp*})\text{Ir(L4)Cl}]\text{PF}_6$ (**Ir4**) with the thermal ellipsoids drawn at the 50% probability level. The hydrogen atoms and PF_6^- counterions have been omitted for clarity. Selected bond lengths (Å) and angles (deg): Ir−C(centroid) = 1.8722, Ir−P = 2.2822(11), Ir−N = 2.116(4), Ir−Cl = 2.3984(11), P−Ir−N = 87.34(10), P−Ir−Cl = 90.00(4), N−Ir−Cl = 83.88(10).

DOI: 10.1021/acs.organomet.9b00080
Organometallics XXXX, XXX, XXX−XXX

pentadienyl (Cp*) ring acting as a three-coordinated ligand, and the monodentate ligand (chloride atom) occupying the sixth coordination site. In addition, the metal center is part of a six-membered (PN)Ir chelate ring system. The Ir−Cl and Ir−Cp*(centroid) distances are 2.3984(11) and 1.8722 Å, respectively. Notably, the Ir−P bond length [Ir−P = 2.2822(11) Å] is longer than Ir−N [Ir−N = 2.116(4) Å].

Stability Studies. Generally, the stability of anticancer metal complexes is a significant factor affecting their functions in biological systems. Thus, the solution's stability in a mixture of 60% dimethyl sulfoxide (DMSO)-d_6/40% D_2O of complexes **Ir1**−**Ir8** was studied by utilizing ^{1}H NMR spectroscopy at a physiological temperature of 310 K. The presence of DMSO-d_6 ensured sufficient solubility of the complex. As illustrated in Figures S33−S40, no change was observed in the ^{1}H NMR spectra over 24 h, thereby indicating that these complexes were stable under such conditions. Complexes **Ir4** and **Ir6** (1.5 mM) were also evaluated for their stability in a 60% DMSO-d_6/40% phosphate-buffered saline (PBS) (pH ≈ 7.2, PBS is prepared from D_2O) buffer mixture by utilizing ^{1}H NMR spectroscopy. As shown in Figures S41 and S42, the ^{1}H NMR spectra of complexes **Ir4** and **Ir6** showed no signals of formation of aqua species, which clearly exhibited that these complexes were stable in PBS buffer solution at 310 K for over 24 h. Complexes **Ir4** and **Ir6** were also monitored over a period of 8 h by ultraviolet/visible (UV/vis) spectroscopy in 10% DMSO/90% PBS (pH ≈ 7.2) at 298 K to further investigate the stability of these complexes (Figures S43 and S44). The results were consistent with the NMR analysis, thereby indicating their sufficient stability in diluted solutions, as is the case of cell culture. Overall, these iridium(III) complexes were stable and remained intact during biological experiments.

In Vitro Cytotoxicity. A number of previous research studies have shown that modifications of the ligand were a contributing factor to toxicological properties of anticancer complexes.[31−36] The in vitro cytotoxicity of complexes **Ir1**−**Ir8** and cisplatin to the human lung cancer cell line (A549) was evaluated by colorimetric MTT assay for 24 h. The IC_{50} values (concentration that produces 50% cell death) are tabulated in Tables 2 and S3 and Figure S45. A majority of complexes were more active than cisplatin to the A549 cells. Notably, complex **Ir8**, showing the most potent activity against A549 cells, displayed approximately 4.5-fold more potent activity than cisplatin. The P^N-chelated complexes in this system showed high cytotoxicity toward A549 cells. For some of the complexes, the cytotoxicity was even higher than those previously reported for P^P and N^N-chelated iridium(III) complexes.[25,26,37]

Within this class, the effect of introducing a biphenyl substituent to the Cp* ring and three types of imine N-substituents in the phosphine-imine framework on the cytotoxicity of these iridium(III) complexes was systematically investigated. First, the aromatic and aliphatic rings of the imine moiety determined the anticancer activity of the complexes. For example, complex **Ir4** (25.3 μM) bearing a cyclohexyl group in the imine moiety displayed lower cytotoxicity than complex **Ir1** (6.5 μM), which contain a phenyl substituent in the same position. Additionally, introducing biphenyl substituents to the Cp* ring optimizes cytotoxicity compared with their parent Cp* complexes (**Ir4**: 25.3 μM vs **Ir7**: 5.8 μM; **Ir6**: 7.9 μM vs **Ir8**: 4.7 μM). Finally, for the two other classes of imine N-substituents, the introduction of ortho alkyl substituents in the aniline and the length of the methylene chain on imine moiety had little influence on the cytotoxicity of these complexes. For example, when the ortho alkyl substituents in aniline increased from the hydrogen atom to the isopropyl group (**Ir1**: 6.5 μM vs **Ir2**: 7.2 μM vs **Ir3**: 6.9 μM) or when the number of the methylene group on the imine moiety increased from 0 to 2 (**Ir1**: 6.5 μM vs **Ir5**: 6.3 μM vs **Ir6**: 7.9 μM), the cytotoxicity exhibited an insignificant change. Overall, the cytotoxicity of these complexes may be primarily attributed to the coordination between iridium(III) and coordinating atoms, and the nature of the imine N-substituents may not be a major factor affecting cytotoxicity.

Table 2. Inhibition of the Growth of A549 Cancer Cells by Complexes Ir1−Ir8 and Cisplatin[a]

complex	IC_{50} (μM)
[(η^5-Cp*)Ir(**L1**)Cl]PF_6 (**Ir1**)	6.5 ± 1.0
[(η^5-Cp*)Ir(**L2**)Cl]PF_6 (**Ir2**)	7.2 ± 2.0
[(η^5-Cp*)Ir(**L3**)Cl]PF_6 (**Ir3**)	6.9 ± 0.6
[(η^5-Cp*)Ir(**L4**)Cl]PF_6 (**Ir4**)	25.3 ± 0.1
[(η^5-Cp*)Ir(**L5**)Cl]PF_6 (**Ir5**)	6.3 ± 0.1
[(η^5-Cp*)Ir(**L6**)Cl]PF_6 (**Ir6**)	7.9 ± 0.9
[(η^5-Cp^{xbiph})Ir(**L4**)Cl]PF_6 (**Ir7**)	5.8 ± 0.2
[(η^5-Cp^{xbiph})Ir(**L6**)Cl]PF_6 (**Ir8**)	4.7 ± 1.5
cisplatin	21.3 ± 1.7

[a]IC_{50} values are drug concentrations necessary for 50% inhibition of cell viability. Data are presented as means ± standard deviations (SDs) and cell viability is assessed after 24 h of incubation.

Reaction with NADH. Half-sandwich Ir(III) anticancer complexes may implicate an oxidant MoA through catalytic hydride transfer from NADH to NAD^+ because this redox pair is involved in relevant redox signaling pathways within cells.[30,38] To evaluate the effect of three different types of N-bound substituents on accelerating the oxidation of NADH to NAD^+, we monitored the conversion reaction of complexes **Ir1**, **Ir3**, **Ir4**, and **Ir6** (1 μM) with NADH (100 μM) in 5% CH_3OH/95% H_2O by using a UV/vis spectrophotometer (Figures 2a and S46). The turnover numbers (TONs) of complexes **Ir1** (19.4), **Ir3** (66.3), **Ir4** (26.6), and **Ir6** (25.4) were calculated based on the difference in absorbance at 339 nm (Figure 2b). Overall, increasing the steric hindrance of ortho-substituents in the aniline enhanced the catalytic activity (**Ir1**: 19.4 vs **Ir3**: 66.3). However, the results for **Ir1**, **Ir4**, and **Ir6** did not allow the clear determination of the influence of the different types of imine N-substituents on catalytic activity. Notably, all tested complexes in this system have more superior catalytic ability in converting coenzyme NADH to NAD^+ (up to 16.2-fold) than the structurally similar half-sandwich iridium(III) complexes containing the P^P-chelating ligand under the same test conditions.[26] The favorable catalytic potency of these complexes in converting NADH to NAD^+ may offer a pathway for generating ROS and may provide efficient oxidant-based therapy.

Interaction with Nucleobases. The study on the reaction of metal anticancer drugs with both mode nucleobase 9-ethylguanine (9-EtG) and 9-methyladenine (9-MeA) provides mechanistic insights into the rationalization of the observed cytotoxicity of these complexes. To assess the nature of interactions of the new iridium(III) complexes **Ir3** and **Ir6** (ca. 1 mM) with 2.0 molar equivalent of mode nucleobase 9-EtG or 9-MeA, we monitored their reactions in 80% CD_3OD/20% D_2O by ^{1}H NMR spectroscopy at 310 K. No additional peaks were observed over a period of 24 h (Figures S47−S50), thereby

DOI: 10.1021/acs.organomet.9b00080
Organometallics XXXX, XXX, XXX−XXX

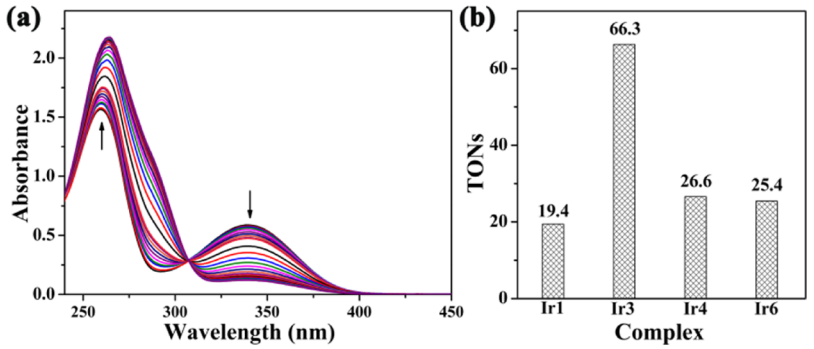

Figure 2. (a) UV/vis spectra of the reaction of complex **Ir3** (1 μM) with NADH (100 μM) in 5% MeOH/95% H_2O (v/v) at 298 K for 8 h. (b) TONs of complexes **Ir1**, **Ir3**, **Ir4**, and **Ir6**.

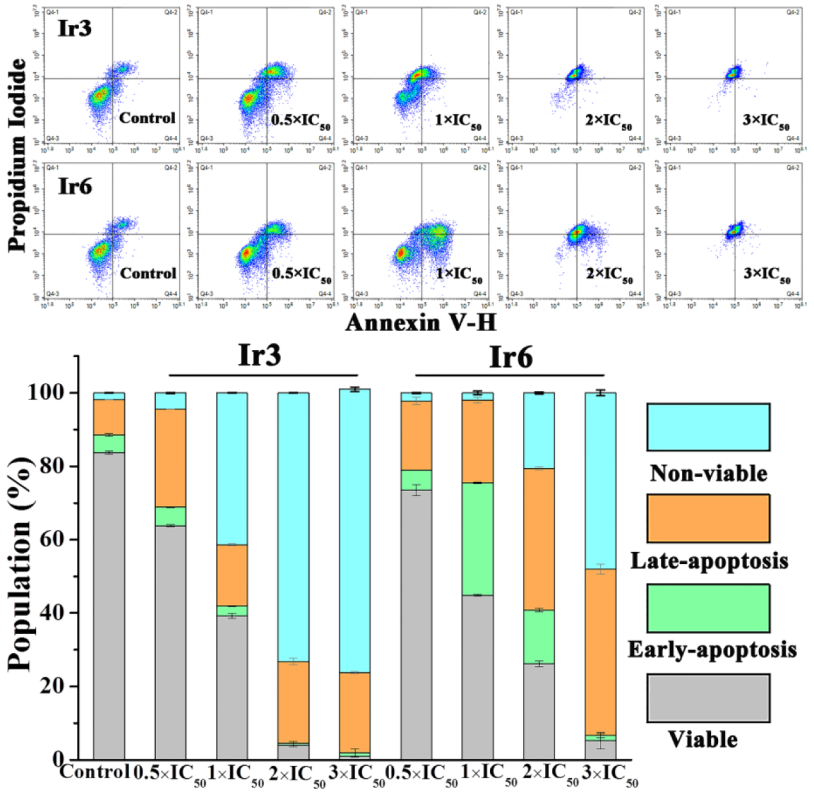

Figure 3. Apoptosis analysis of A549 cells after 24 h of exposure to complexes **Ir3** and **Ir6** at 310 K determined by flow cytometry using AV-fluorescein isothiocyanate versus PI staining. Populations for cells in four stages treated by complexes **Ir3** and **Ir6**. Data are quoted as mean ± SD of three replicates.

indicating that no reaction with 9-EtG and 9-MeA occurred. Additionally, these reaction mixtures were analyzed by mass spectrometry. The formation of nucleobase adducts was not detected. Hence, potential DNA target sites are not prone to attack from these half-sandwich iridium(III) complexes.

Apoptosis Assay. To evaluate whether such complexes lead to cell death through apoptosis or necrosis, we carried out annexin V (AV)/propidium iodide (PI) dual-staining in A549 cells after incubation with complexes **Ir3** and **Ir6** for 24 h. As shown in Figure 3 and Tables S4 and S5, following incubation with complexes **Ir3** and **Ir6** at concentrations of 0.5 × IC_{50}, 1 × IC_{50}, 2 × IC_{50}, and 3 × IC_{50}, distinct apoptosis and necrosis were observed. As indicated in the histogram, when A549 cells were treated with test complexes at low concentrations, most of the cells underwent apoptosis. However, when the test complex at high concentrations was used, a dose-related increase in the percentage of necrosis was detected. At the maximum concentration (3 × IC_{50}) of complexes **Ir3** and **Ir6**, 20.73 and 45.35% of cells underwent late apoptosis, respectively, which were higher compared with the control group (9.64%). Additionally, the percentages of cells that underwent necrosis were 77.23 and 47.99% at 3 × IC_{50}, respectively, which were higher compared with the vehicle-treated group (1.85%). These results indicated that cell death occurred because of apoptosis and necrosis.

Mitochondrial Membrane Potential. The mitochondria play crucial roles in activating cell apoptosis. The change of mitochondrial membrane potential (MMP) ($\Delta\psi_m$) is one of the earliest events in apoptosis. Hence, $\Delta\psi_m$ should be monitored when cell apoptosis starts. The influence of iridium(III) complexes on MMP was examined by staining with a lipophilic cationic fluorescent probe, 5,5′,6,6′-tetrachloro-1,1′,3,3′-tetrae-

DOI: 10.1021/acs.organomet.9b00080
Organometallics XXXX, XXX, XXX−XXX

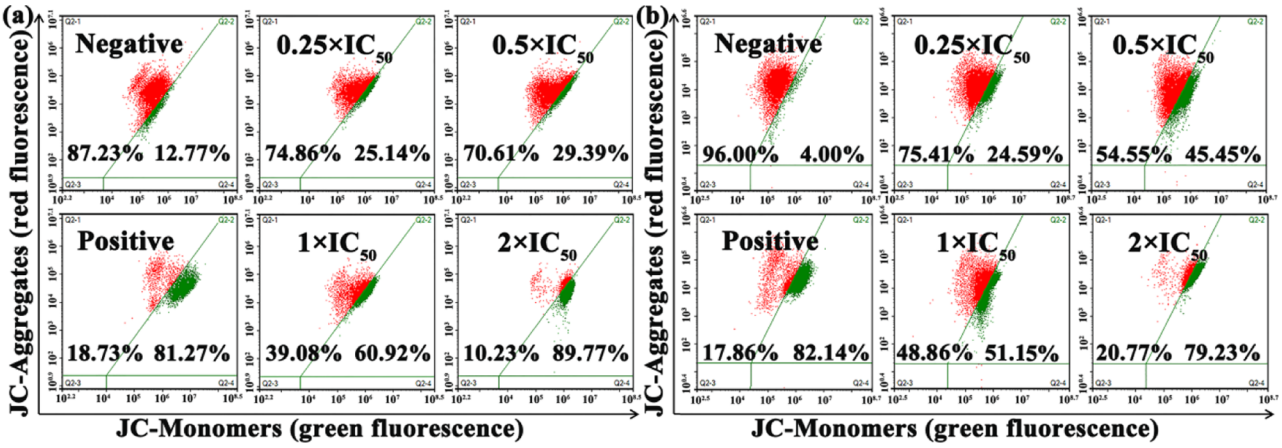

Figure 4. Changes in MMP of A549 cancer cells induced by complexes **Ir3** (a) and **Ir6** (b).

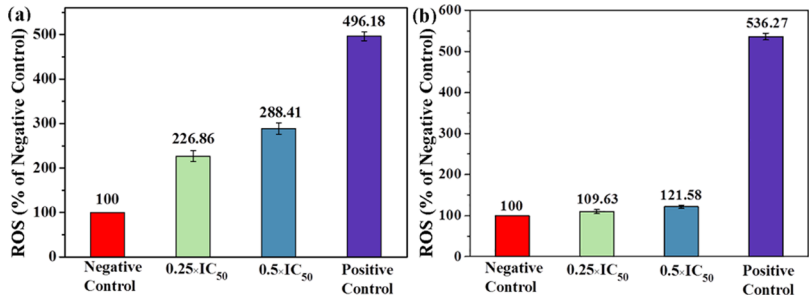

Figure 5. Analysis of ROS levels through flow cytometry after A549 cells were treated with complexes **Ir3** (a) and **Ir6** (b) at the concentrations of 0.25 × IC_{50} and 0.5 × IC_{50} for 24 h and stained with H_2DCFDA.

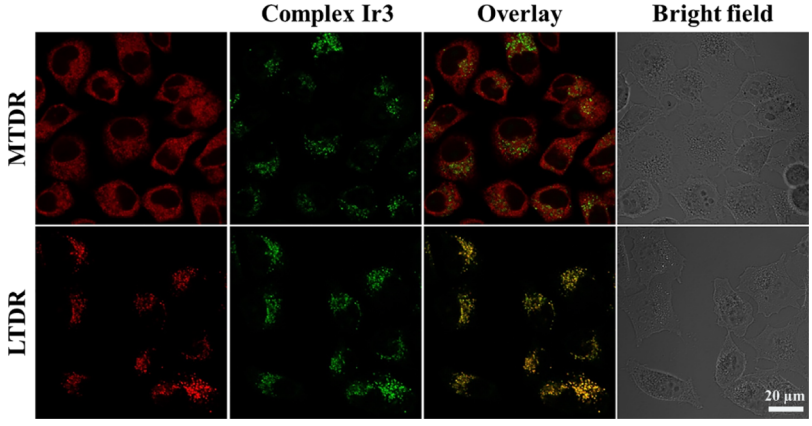

Figure 6. Confocal microscopy images of A549 cells co-labeled with **Ir3** (10 μM, 1 h) and MTDR (500 nM, 20 min) or LTDR (75 nM, 20 min) at 37 °C. **Ir3** (λ_{ex}: 488 nm, λ_{em}: 520 ± 30 nm); MTDR (λ_{ex}: 644 nm, λ_{em}: 700 ± 30 nm); LTDR (λ_{ex}: 594 nm, λ_{em}: 630 ± 30 nm). Scale bar: 20 μm.

thylbenzimidazolylcarbocyanine iodide (JC-1). As depicted in Figures 4 and S5, and Tables S6 and S7. A549 cells were treated with complexes **Ir3** and **Ir6** at 0.25, 0.5, 1.0, and 2.0 equivalents of IC_{50} for 24 h, followed by staining with JC-1 and analysis by flow cytometry. A substantial dose-related red-to-green color shift was observed, thereby suggesting MMP loss. The percentage of depolarized cells increased from 12.77 to 89.77% and 4.00 to 79.23% for **Ir3** and **Ir6** at 2 × IC_{50}, respectively. Hence, the loss of MMP may be an apoptotic mediating factor.

ROS Determination. The increase of the intracellular ROS level is a well-known MoA.[39,40] This family of complexes triggers the formation of intracellular ROS in A549 cancer cells and was evaluated via flow cytometry by utilizing 2′,7′-dichlorofluorescein diacetate (H_2DCFDA) staining. Intracellular ROS can promote conversion of nonfluorescent H_2DCFDA to the fluorescent product 2′,7′-dichlorofluorescein (DCF).[41] As illustrated in Figures 5 and S52, compared with the control group, the DCF intensity indicated a concentrate-dependent increase upon treatment with complexes **Ir3** and **Ir6** at concentrations of approximately 0.25 × IC_{50} value and 0.5 × IC_{50} value for 24 h, respectively. The increased ROS level for these complexes played an important role in their anticancer activity and was deemed as the MoA in this system. Notably, similar half-sandwich C,N-chelating iridium anticancer complexes were used to generate the ROS by catalytic hydride transfer from the coenzyme NADH to oxygen.[30] As a result, the ROS level elevation may be attributed to the conversion of

DOI: 10.1021/acs.organomet.9b00080
Organometallics XXXX, XXX, XXX−XXX

NADH to NAD^+ by these complexes, which was also observed in this system. In addition, in the "reaction with NADH" section, **Ir6** showed a lower catalytic ability in converting coenzyme NADH to NAD^+ than **Ir3** (**Ir6**: 25.4 vs **Ir3**: 66.3). This result is consistent with **Ir6**'s lower ROS level elevation compared with **Ir3**. Therefore, the ROS level elevation is correlated with the conversion of NADH to NAD^+ in this system.

Intracellular Localization. The cellular localization of anticancer metallodrugs can be visualized by employing confocal microscopy imaging due to their intrinsic emission properties.[42,43] To understand which organelles would be targeted by these iridium(III) complexes, we performed colocalization experiments of **Ir3** and LysoTracker Deep Red (LTDR) or MitoTracker Deep Red (MTDR) within A549 cells by employing confocal microscopy. As shown in Figure 6, **Ir3** efficiently accumulates in A549 cells after 1 h of incubation and exhibits an intense and punctate staining pattern as a result of its compartmentalization. Co-localization analysis with the lysosome dye LTDR (75 nM) displays that **Ir3** (10 μM) selectively accumulates in lysosomes. The Pearson's colocalization coefficients obtained for **Ir3** with LTDR was 72 ± 2%. Negligible colocalization was observed for **Ir3** with the MTDR. These results indicated that **Ir3** can specifically distribute in the lysosomes.

Lysosomal Damage. Lysosomes are membrane-bound organelles, which are involved in many physiological processes.[44−46] To assess whether lysosomal damage was the pathway of cell death, we utilized acridine orange as a probe to evaluate the dysfunction of lysosomes. Acridine orange is the most reported and commercially available LysoTrackers because it emits red fluorescence in lysosomes and green fluorescence in the cytosol and nuclei.[47,48] As illustrated in Figure 7a, A549 cells

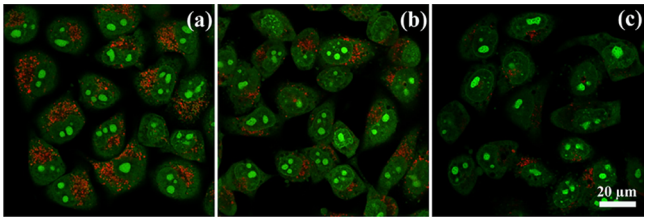

Figure 7. Confocal luminescence imaging of acridine orange (5 μM) stained A549 cells after different treatments. (a) Only acridine orange; (b) acridine orange and complex **Ir3** (1 × IC_{50}); (c) acridine orange and complex **Ir3** (2 × IC_{50}). λ_{ex}: 488 nm; λ_{em}: 490−530 nm (green channel); 605−645 nm (red channel). Scale bars: 20 μm.

alone treated with acridine orange (5 μM) showed red fluorescence in the lysosomes, thereby indicating that the lysosomes of A549 cells were intact under such conditions. When the A549 cells were treated with complex **Ir3** at 1 × IC_{50} and 2 × IC_{50}, the red fluorescence of acridine orange severely decreased in a dose-dependent manner (Figure 7b,c), thereby suggesting that lysosomal integrity was disrupted. Hence, complex **Ir3** may induce cell death via the disruption of lysosomes.

Cellular Uptake Mechanisms. These complexes crossed the membrane rapidly and preferentially accumulated in the perinuclear region. Therefore, the cellular uptake mechanisms of drug molecules were investigated by confocal microscopy. A549 cells were treated with **Ir3** at lower temperature (4 °C), or 37 °C, or upon pretreatment with different inhibitors (energy inhibitor carbonyl cyanide *m*-chlorophenyl hydrazone and the endocytosis inhibitor chloroquine). As indicated in Figure S53, no distinct alteration of the luminescent intensity in the three experiment groups were observed compared with the vehicle-treated group (37 °C), thereby suggesting that **Ir3** entered A549 cells via a non-energy-dependent pathway. Notably, the previously reported half-sandwich iridium(III) complexes with P^P chelating ligands showed different cellular uptake mechanisms (an energy-dependent pathway) from these complexes.[49]

CONCLUSIONS

A series of novel half-sandwich iridium(III) complexes containing various phosphine-imine ligands were successfully synthesized and fully characterized. Stability studies revealed that the chemical composition of these complexes in aqueous media and in DMSO solutions did not change in the biological experiments. Most of these complexes displayed high cytotoxicity for the A549 cell line, distinctly surpassing the cisplatin activity in this cell type. Replacing the cyclohexyl group in the imine moiety with a phenyl group enhanced the cytotoxicity. Moreover, the introduction of biphenyl substituents onto the Cp* ring optimized cytotoxicity compared with their parent Cp* complexes. Additionally, the ortho alkyl substituents in aniline and the length of the methylene chain on the imine moiety did not affect the cytotoxicity of the complexes. The cytotoxicity of these complexes may be primarily attributed to the coordination between iridium(III) and coordinating atoms, and the nature of the imine N-substituents may not be a major factor affecting cytotoxicity. Cell death mechanism studies indicated that these complexes caused cell apoptosis and necrosis, generated ROS, and disrupted the MMP. Further mechanism studies through confocal microscopy showed that this class of complexes was taken up via non-energy-dependent mechanisms and mainly gathered in the lysosomes in A549 cancer cells. The disruption of lysosomes was also responsible for cell death. These preliminary results implied that this work may be helpful for the development and design of potential anticancer complexes with mixed P/N-based chelating ligands.

EXPERIMENTAL SECTION

Chemicals and Reagents. $IrCl_3 \cdot nH_2O$, 1,2,3,4,5-pentamethylcyclopentadiene (95%), butyllithium solution (1.6 M in hexane), 2,3,4,5-tetramethyl-2-cyclopentenone (95%), 4-bromo-biphenyl, 2-diphenylphosphinobenzaldehyde, aniline, 2,6-dimethylaniline, 2,6-diisopropylaniline, cyclohexylamine, benzylamine, 2-phenylethylamine, 9-EtG, 9-MeA, and reduced form of nicotinamide-adenine dinucleotid (NADH) were purchased from commercial sources and used without further purification. $[(\eta^5\text{-Cp*})IrCl_2]_2$ (**dimer 1**) and $[(\eta^5\text{-Cp}^{xbiph})\text{-}IrCl_2]_2$ (**dimer 2**) were prepared by a method in the literature.[50] The phosphine-imine ligands (**L1**−**L6**) were obtained through a Schiff-base condensation reaction previously reported.[51−57]

Synthesis of the Complexes. *General Method.* A mixture of the phosphine-imine ligand (0.10 mmol) and $[(\eta^5\text{-Cp}^x)IrCl_2]_2$ (0.05 mmol) was dissolved in CH_2Cl_2 (20 mL) and stirred at room temperature for 20 h. Then, solid KPF_6 (0.60 mmol) was added with stirring. After 2 h, KPF_6 was filtered off. The solvent was removed under reduced pressure. The resulting solid was purified by recrystallization, providing orange crystals.

$[(\eta^5\text{-Cp*})Ir(\mathbf{L1})Cl]PF_6$ (**Ir1**) yield: 47 mg (54%). ^1H NMR (500 MHz, DMSO): δ 8.62 (d, J = 2.4 Hz, 1H, *H*C═N), 7.87−7.80 (m, 3H, Ar-*H*), 7.72 (ddt, J = 18.3, 15.9, 7.8 Hz, 11H, Ar-*H*), 7.62 (t, J = 7.6 Hz, 1H, Ar-*H*), 7.49 (dd, J = 10.6, 7.8 Hz, 1H, Ar-*H*), 7.41 (t, J = 7.5 Hz, 1H, Ar-*H*), 7.12 (d, J = 7.7 Hz, 2H, Ar-*H*), 1.02 (d, J = 2.3 Hz, 15H, Cp*-*H*). ^{31}P NMR (202 MHz, DMSO): δ 11.41 (s), −133.65 (s), −137.17 (s), −140.68 (s), −144.19 (s), −147.71 (s), −151.22 (s), −154.73 (s). FT-

DOI: 10.1021/acs.organomet.9b00080
Organometallics XXXX, XXX, XXX−XXX

IR (KBr disk, cm^{-1}): ν(C═N imine) 1568.9. MALDI-TOF-MS (m/z): calcd for $C_{35}H_{35}ClIrPN$, 728.1825; found, 728.1370 [(η^5-Cp*)Ir(**L1**)Cl]$^+$. Elemental analysis calcd (%) for $C_{35}H_{35}NClIrP_2F_6$: C, 48.14; H, 4.04; N, 1.60. Found: C, 48.29; H, 4.08; N, 1.65.

[(η^5-Cp*)Ir(**L2**)Cl]PF_6 (**Ir2**) yield: 63 mg (70%). ^{1}H NMR (500 MHz, $CDCl_3$): δ 8.07 (d, J = 3.2 Hz, 1H, *HC*═N), 7.72−7.65 (m, 4H, Ar-*H*), 7.64−7.58 (m, 5H, Ar-*H*), 7.54 (td, J = 8.0, 2.8 Hz, 2H, Ar-*H*), 7.28 (d, J = 3.8 Hz, 1H, Ar-*H*), 7.23 (s, 1H, Ar-*H*), 7.18 (d, J = 6.9 Hz, 1H, Ar-*H*), 7.07−7.00 (m, 3H, Ar-*H*), 2.27 (s, 3H, *o*-aniline-CH_3), 1.37 (s, 3H, *o*-aniline-CH_3), 1.16 (d, J = 2.4 Hz, 15H, Cp*-*H*). ^{31}P NMR (202 MHz, $CDCl_3$): δ 6.64 (s), −133.94 (s), −137.46 (s), −140.98 (s), −144.50 (s), −148.02 (s), −151.53 (s), −155.05 (s). FT-IR (KBr disk, cm^{-1}): ν(C═N imine) 1602.0. MALDI-TOF-MS (m/z): calcd for $C_{37}H_{39}ClIrPN$, 756.2138; found, 756.1720 [(η^5-Cp*)Ir(**L2**)Cl]$^+$. Elemental analysis calcd (%) for $C_{37}H_{39}NClIrP_2F_6$: C, 49.30; H, 4.36; N, 1.55. Found: C, 49.49; H, 4.42; N, 1.58.

[(η^5-Cp*)Ir(**L3**)Cl]PF_6 (**Ir3**) yield: 44 mg (46%). ^{1}H NMR (500 MHz, $CDCl_3$): δ 8.07 (d, J = 2.9 Hz, 1H, *HC*═N), 7.68 (tt, J = 14.9, 7.4 Hz, 5H, Ar-*H*), 7.63−7.59 (m, 1H, Ar-*H*), 7.51 (dd, J = 6.7, 4.6 Hz, 4H, Ar-*H*), 7.34−7.27 (m, 3H, Ar-*H*), 7.24 (d, J = 7.8 Hz, 2H, Ar-*H*), 7.16−7.03 (m, 2H, Ar-*H*), 3.46−3.43 (m, 1H, ^{i}Pr-C*H*), 2.19−2.12 (m, 1H, ^{i}Pr-C*H*), 1.38 (d, J = 6.8 Hz, 3H, ^{i}Pr-CH_3), 1.19 (d, J = 2.4 Hz, 15H, Cp*-*H*), 1.10 (d, J = 6.6 Hz, 3H, ^{i}Pr-CH_3), 1.06 (d, J = 6.7 Hz, 3H, ^{i}Pr-CH_3), 0.18 (d, J = 6.6 Hz, 3H, ^{i}Pr-CH_3). ^{31}P NMR (202 MHz, $CDCl_3$): δ 6.89 (s), −133.94 (s), −137.46 (s), −140.98 (s), −144.50 (s), −148.02 (s), −151.54 (s), 155.06 (s). FT-IR (KBr disk, cm^{-1}): ν(C═N imine) 1599.0. MALDI-TOF-MS (m/z): calcd for $C_{41}H_{47}ClIrPN$, 812.2764; found, 812.1550 [(η^5-Cp*)Ir(**L3**)Cl]$^+$. Elemental analysis calcd (%) for $C_{41}H_{47}NClIrP_2F_6$: C, 51.43; H, 4.95; N, 1.46. Found: C, 51.38; H, 4.83; N, 1.54.

[(η^5-Cp*)Ir(**L4**)Cl]PF_6 (**Ir4**) yield: 58 mg (66%). ^{1}H NMR (500 MHz, DMSO): δ 8.64 (d, J = 2.5 Hz, 1H, *HC*═N), 7.82 (dd, J = 7.3, 3.8 Hz, 1H, Ar-*H*), 7.75−7.53 (m, 12H, Ar-*H*), 7.46 (dd, J = 10.0, 8.0 Hz, 1H, Ar-*H*), 4.03 (t, J = 11.8 Hz, 1H, Cy-*H*), 1.95 (t, J = 11.7 Hz, 2H, Cy-*H*), 1.84 (d, J = 13.3 Hz, 1H, Cy-*H*), 1.75 (t, J = 12.2 Hz, 2H, Cy-*H*), 1.68 (d, J = 12.5 Hz, 1H, Cy-*H*), 1.63−1.53 (m, 1H, Cy-*H*), 1.53−1.47 (m, 1H, Cy-*H*), 1.44 (d, J = 14.1 Hz, 1H, Cy-*H*), 1.40 (d, J = 2.1 Hz, 15H, Cp*-*H*), 1.23 (dd, J = 25.8, 12.8 Hz, 1H, Cy-*H*). ^{31}P NMR (202 MHz, DMSO): δ 12.32 (s), −133.65 (s), −137.17 (s), −140.68 (s), −144.19 (s), −147.71 (s), −151.22 (s), −154.73 (s). FT-IR (KBr disk, cm^{-1}): ν(C═N imine) 1617.4. MALDI-TOF-MS (m/z): calcd for $C_{35}H_{41}ClIrPN$, 734.2294; found, 734.1700 [(η^5-Cp*)Ir(**L4**)Cl]$^+$. Elemental analysis calcd (%) for $C_{35}H_{41}NClIrP_2F_6$: C, 47.81; H, 4.70; N, 1.59. Found: C, 47.96; H, 4.80; N, 1.53. Crystals of complex **Ir4** qualified for X-ray analysis were obtained by slow diffusion of hexane into a concentrated solution of complex **Ir4** in dichloromethane.

[(η^5-Cp*)Ir(**L5**)Cl]PF_6 (**Ir5**) yield: 53 mg (60%). ^{1}H NMR (500 MHz, $CDCl_3$): δ 8.11 (d, J = 1.7 Hz, 1H, *HC*═N), 7.63 (dd, J = 13.1, 7.3 Hz, 6H, Ar-*H*), 7.59−7.48 (m, 6H, Ar-*H*), 7.42 (td, J = 7.8, 2.7 Hz, 2H, Ar-*H*), 7.30−7.27 (m, 3H, Ar-*H*), 7.21−7.16 (m, 2H, Ar-*H*), 5.43 (d, J = 15.4 Hz, 1H, ArCH_2N), 5.30 (d, J = 15.4 Hz, 1H, ArCH_2N), 1.41 (s, 15H, Cp*-*H*). ^{31}P NMR (202 MHz, $CDCl_3$): δ 8.02 (s), −133.70 (s), −137.22 (s), −140.74 (s), −144.26 (s), −147.78 (s), −151.30 (s), −154.82 (s). FT-IR (KBr disk, cm^{-1}): ν(C═N imine) 1614.7. MALDI-TOF-MS (m/z): calcd for $C_{36}H_{37}ClIrPN$, 742.1981; found, 742.1977 [(η^5-Cp*)Ir(**L5**)Cl]$^+$. Elemental analysis calcd (%) for $C_{36}H_{37}NClIrP_2F_6$: C, 48.73; H, 4.20; N, 1.58. Found: C, 48.63; H, 4.25; N, 1.63.

[(η^5-Cp*)Ir(**L6**)Cl]PF_6 (**Ir6**) yield: 70 mg (78%). ^{1}H NMR (500 MHz, DMSO): δ 8.29 (d, J = 1.8 Hz, 1H, *HC*═N), 7.76 (t, J = 7.6 Hz, 1H, Ar-*H*), 7.73−7.61 (m, 6H, Ar-*H*), 7.57 (dt, J = 8.9, 3.5 Hz, 6H, Ar-*H*), 7.48 (dd, J = 7.3, 3.7 Hz, 1H, Ar-*H*), 7.29 (dd, J = 11.1, 4.4 Hz, 2H, Ar-*H*), 7.24 (dd, J = 6.2, 3.9 Hz, 1H, Ar-*H*), 7.23−7.17 (m, 2H, Ar-*H*), 4.53−4.41 (m, 1H, ArCH_2CH_2N), 4.28−4.17 (m, 1H, ArCH_2CH_2N), 2.71 (ddd, J = 13.4, 8.3, 5.0 Hz, 1H, ArCH_2CH$_2$N), 2.58 (dt, J = 13.7, 8.1 Hz, 1H, ArCH_2CH$_2$N), 1.38 (s, 15H, Cp*-*H*). ^{31}P NMR (202 MHz, DMSO): δ 8.09 (s), −133.65 (s), −137.16 (s), −140.68 (s), −144.19 (s), −147.70 (s), −151.22 (s), −154.73 (s). FT-IR (KBr disk, cm^{-1}): ν(C═N imine) 1611.9. MALDI-TOF-MS (m/z): calcd for $C_{37}H_{39}ClIrPN$, 756.2138; found, 756.2055 [(η^5-Cp*)Ir(**L6**)Cl]$^+$. Elemental analysis calcd (%) for $C_{37}H_{39}NClIrP_2F_6$: C, 49.30; H, 4.36; N, 1.55. Found: C, 49.11; H, 4.29; N, 1.49.

[(η^5-Cp^{xbiph})Ir(**L4**)Cl]PF_6 (**Ir7**) yield: 63 mg (62%). ^{1}H NMR (500 MHz, DMSO): δ 8.61 (s, 1H, *HC*═N), 7.85−7.80 (m, 3H, Ar-*H*), 7.75−7.70 (m, 5H, Ar-*H*), 7.69−7.60 (m, 11H, Ar-*H*), 7.54−7.49 (m, 3H, Ar-*H*), 7.43 (t, J = 7.4 Hz, 1H, Ar-*H*), 3.66 (t, J = 11.7 Hz, 1H, Cy-*H*), 2.23 (s, 3H, Cp^{xbiph}-CH_3), 1.98 (d, J = 11.7 Hz, 1H, Cy-*H*), 1.68 (s, 2H, Cy-*H*), 1.66−1.57 (m, 4H, Cy-*H* and Cp^{xbiph}-CH_3), 1.54 (d, J = 1.7 Hz, 3H, Cp^{xbiph}-CH_3), 1.45 (dt, J = 21.1, 7.3 Hz, 1H, Cy-*H*), 1.30 (d, J = 10.7 Hz, 2H, Cy-*H*), 1.03−0.93 (m, 2H, Cy-*H*), 0.30 (s, 3H, Cp^{xbiph}-CH_3), −0.13 (dt, J = 22.1, 11.0 Hz, 1H, Cy-*H*). ^{31}P NMR (202 MHz, DMSO): δ 12.29 (s), −133.65 (s), −137.16 (s), −140.68 (s), −144.19 (s), −147.70 (s), −151.22 (s), −154.73 (s). FT-IR (KBr disk, cm^{-1}): ν(C═N imine) 1616.8. MALDI-TOF-MS (m/z): calcd for $C_{46}H_{47}ClIrPN$, 872.2764; found, 872.2042 [(η^5-Cp^{xbiph})Ir(**L4**)Cl]$^+$. Elemental analysis calcd (%) for $C_{46}H_{47}NClIrP_2F_6$: C, 54.30; H, 4.66; N, 1.38. Found: C, 54.46; H, 4.69; N, 1.39.

[(η^5-Cp^{xbiph})Ir(**L6**)Cl]PF_6 (**Ir8**) yield: 53 mg (51%). ^{1}H NMR (500 MHz, DMSO): δ 8.79 (d, J = 1.9 Hz, 1H, *HC*═N), 7.94−7.70 (m, 9H, Ar-*H*), 7.65−7.29 (m, 14H, Ar-*H*), 7.24−7.11 (m, 3H, Ar-*H*), 6.96−6.88 (m, 2H, Ar-*H*), 4.30 (td, J = 11.6, 5.8 Hz, 1H, ArCH$_2$CH_2N), 4.13 (td, J = 11.6, 4.8 Hz, 1H, ArCH$_2$CH_2N), 3.20 (td, J = 12.0, 5.2 Hz, 1H, ArCH_2CH$_2$N), 2.43 (td, J = 12.0, 4.2 Hz, 1H, ArCH_2CH$_2$N), 1.93 (d, J = 1.7 Hz, 3H, Cp^{xbiph}-CH_3), 1.70 (d, J = 3.9 Hz, 3H, Cp^{xbiph}-CH_3), 1.49 (d, J = 3.0 Hz, 3H, Cp^{xbiph}-CH_3), 0.53 (s, 3H, Cp^{xbiph}-CH_3). ^{31}P NMR (202 MHz, DMSO): δ 7.08 (s), −133.66 (s), −137.17 (s), −140.68 (s), −144.20 (s), −147.71 (s), −151.22 (s), −154.73 (s). FT-IR (KBr disk, cm^{-1}): ν(C═N imine) 1616.8. MALDI-TOF-MS (m/z): calcd for $C_{48}H_{45}ClIrPN$, 894.2607; found, 894.2693 [(η^5-Cp^{xbiph})Ir(**L6**)Cl]$^+$. Elemental analysis calcd (%) for $C_{48}H_{45}NClIrP_2F_6$: C, 55.46; H, 4.36; N, 1.35. Found: C, 55.60; H, 4.44; N, 1.30.

■ ASSOCIATED CONTENT

Supporting Information

The Supporting Information is available free of charge on the ACS Publications website at DOI: 10.1021/acs.organomet.9b00080.

Details of the Experimental Section, ^{1}H NMR spectrum, ^{31}P NMR spectrum, FT-IR spectra, MALDI-TOF-MS, UV/vis spectrum and ^{1}H NMR spectra for stability studies, low-field region of the ^{1}H NMR spectra for reactions of complexes **Ir3** and **Ir6** with nucleobases, analysis of ROS levels, confocal images of A549 cells, and crystallographic data for complex **Ir4** (CCDC number: 1877562) (PDF)

Accession Codes

CCDC 1877562 contains the supplementary crystallographic data for this paper. These data can be obtained free of charge via www.ccdc.cam.ac.uk/data_request/cif, or by emailing data_request@ccdc.cam.ac.uk, or by contacting The Cambridge Crystallographic Data Centre, 12 Union Road, Cambridge CB2 1EZ, UK; fax: +44 1223 336033.

■ AUTHOR INFORMATION

Corresponding Authors

*E-mail: guolihua@qfnu.edu.cn (L.G.).
*E-mail: liuzheqd@163.com (Z.L.).

ORCID

Lihua Guo: 0000-0002-0842-9958
Zhe Liu: 0000-0001-5796-4335

Notes

The authors declare no competing financial interest.

DOI: 10.1021/acs.organomet.9b00080
Organometallics XXXX, XXX, XXX−XXX

■ ACKNOWLEDGMENTS

We thank Shandong Provincial Natural Science Foundation (ZR2018MB023), the National Natural Science Foundation of China (grant no. 21671118) and the Taishan Scholars Program, The Key Laboratory of Polymeric Composite & Functional Materials of Ministry of Education (PCFM-2017-01), Excellent experiment project of Qufu Normal University (jp201705).

■ REFERENCES

(1) Siegel, R. L.; Miller, K. D.; Jemal, A. Cancer statistics, 2018. *Ca-Cancer J. Clin.* **2018**, *68*, 7−30.
(2) Florea, A.-M.; Büsselberg, D. Cisplatin as an anti-tumor drug: cellular mechanisms of activity, drug resistance and induced side effects. *Cancers* **2011**, *3*, 1351−1371.
(3) Wang, D.; Lippard, S. J. Cellular processing of platinum anticancer drugs. *Nat. Rev. Drug Discovery* **2005**, *4*, 307−320.
(4) Wang, X.; Wang, X.; Jin, S.; Muhammad, N.; Guo, Z. Stimuli-responsive therapeutic metallodrugs. *Chem. Rev.* **2019**, *119*, 1138−1192.
(5) Dasari, S.; Bernard Tchounwou, P. Cisplatin in cancer therapy: molecular mechanisms of action. *Eur. J. Pharmacol.* **2014**, *740*, 364−378.
(6) Mehmood, R. K. Review of Cisplatin and oxaliplatin in current immunogenic and monoclonal antibody treatments. *Oncol. Rev.* **2014**, *8*, 256.
(7) Ho, G. Y.; Woodward, N.; Coward, J. I. G. Cisplatin versus carboplatin: comparative review of therapeutic management in solid malignancies. *Crit. Rev. Oncol. Hematol.* **2016**, *102*, 37−46.
(8) Oun, R.; Moussa, Y. E.; Wheate, N. J. The side effects of platinum-based chemotherapy drugs: a review for chemists. *Dalton Trans.* **2018**, *47*, 6645−6653.
(9) Yang, Y.; Guo, L.; Ge, X.; Tian, Z.; Gong, Y.; Zheng, H.; Du, Q.; Zheng, X.; Liu, Z. Novel lysosome-targeted cyclometalated iridium(III) anticancer complexes containing imine-N-heterocyclic carbene ligands: synthesis, spectroscopic properties and biological activity. *Dyes Pigm.* **2019**, *161*, 119−129.
(10) Guo, L.; Dai, S.; Sui, X.; Chen, C. Palladium and nickel catalyzed chain walking olefin polymerization and copolymerization. *ACS Catal.* **2016**, *6*, 428−441.
(11) Liang, T.; Chen, C. Position makes the difference: electronic effects in nickel-catalyzed ethylene polymerizations and copolymerizations. *Inorg. Chem.* **2018**, *57*, 14913−14919.
(12) Guo, L.; Zou, C.; Dai, S.; Chen, C. Direct Synthesis of Branched Carboxylic Acid Functionalized Poly(1-octene) by α-Diimine Palladium Catalysts. *Polymers* **2017**, *9*, 122.
(13) Xiong, S.; Guo, L.; Zhang, S.; Liu, Z. Asymmetric cationic [P, O] type palladium complexes in olefin homopolymerization and copolymerization. *Chin. J. Chem.* **2017**, *35*, 1209−1221.
(14) Guo, L.; Lian, K.; Kong, W.; Xu, S.; Jiang, G.; Dai, S. Synthesis of various branched ultra-high-molecular-weight polyethylenes using sterically hindered acenaphthene-based α-diimine Ni(II) catalysts. *Organometallics* **2018**, *37*, 2442−2449.
(15) Guo, L.; Liu, Y.; Sun, W.; Du, Q.; Yang, Y.; Kong, W.; Liu, Z.; Chen, D. Synthesis, characterization, and olefin (co)polymerization behavior of unsymmetrical α-diimine palladium complexes containing bulky substituents at 4-position of aniline moieties. *J. Organomet. Chem.* **2018**, *877*, 12−20.
(16) Konkankit, C. C.; Marker, S. C.; Knopf, K. M.; Wilson, J. J. Anticancer activity of complexes of the third row transition metals, rhenium, osmium, and iridium. *Dalton Trans.* **2018**, *47*, 9934−9974.
(17) Notaro, A.; Gasser, G. Monomeric and dimeric coordinatively saturated and substitutionally inert Ru(II) polypyridyl complexes as anticancer drug candidates. *Chem. Soc. Rev.* **2017**, *46*, 7317−7337.
(18) Guerriero, A.; Oberhauser, W.; Riedel, T.; Peruzzini, M.; Dyson, P. J.; Gonsalvi, L. New class of half-sandwich ruthenium(II) arene complexes bearing the water-soluble CAP ligand as an in vitro anticancer agent. *Inorg. Chem.* **2017**, *56*, 5514−5518.
(19) Zeng, L.; Gupta, P.; Chen, Y.; Wang, E.; Ji, L.; Chao, H.; Chen, Z.-S. The development of anticancer ruthenium(II) complexes: from single molecule compounds to nanomaterials. *Chem. Soc. Rev.* **2017**, *46*, 5771−5804.
(20) Zou, T.; Lum, C. T.; Lok, C.-N.; Zhang, J.-J.; Che, C.-M. Chemical biology of anticancer gold(III) and gold(I) complexes. *Chem. Soc. Rev.* **2015**, *44*, 8786−8801.
(21) Yang, Y.; Ge, X.; Guo, L.; Zhu, T.; Tian, Z.; Zhang, H.; Du, Q.; Peng, H.; Ma, W.; Liu, Z. Zwitterionic and cationic half-sandwich iridium(III) ruthenium(II) complexes bearing sulfonate groups: synthesis, characterization and their different biological activities. *Dalton Trans.* **2019**, *48*, 3193−3197.
(22) Srinivasa Reddy, T.; Privér, S. H.; Mirzadeh, N.; Bhargava, S. K. Synthesis of gold(I) phosphine complexes containing the 2-$BrC_6F_4PPh_2$ ligand: Evaluation of anticancer activity in 2D and 3D spheroidal models of HeLa cancer cells. *Eur. J. Med. Chem.* **2018**, *145*, 291−301.
(23) Brissos, R. F.; Clavero, P.; Gallen, A.; Grabulosa, A.; Barrios, L. A.; Caballero, A. B.; Korrodi-Gregório, L.; Pérez-Tomás, R.; Muller, G.; Soto-Cerrato, V.; Gamez, P. Highly cytotoxic ruthenium(II)-arene complexes from bulky 1-pyrenylphosphane ligands. *Inorg. Chem.* **2018**, *57*, 14786−14797.
(24) Clemente, M.; Polat, I. H.; Albert, J.; Bosque, R.; Crespo, M.; Granell, J.; López, C.; Martínez, M.; Quirante, J.; Messeguer, R.; Calvis, C.; Badía, J.; Baldomà, L.; Font-Bardia, M.; Cascante, M. Platinacycles containing a primary amine platinum(II) compounds for treating cisplatin-resistant cancers by oxidant therapy. *Organometallics* **2018**, *37*, 3502−3514.
(25) Biancalana, L.; Batchelor, L. K.; Funaioli, T.; Zacchini, S.; Bortoluzzi, M.; Pampaloni, G.; Dyson, P. J.; Marchetti, F. α-diimines as versatile, derivatizable ligands in ruthenium(II) *p*-cymene anticancer complexes. *Inorg. Chem.* **2018**, *57*, 6669−6685.
(26) Li, J.; Tian, M.; Tian, Z.; Zhang, S.; Yan, C.; Shao, C.; Liu, Z. Half-sandwich iridium(III) and ruthenium(II) complexes containing P^P-chelating ligands: A new class of potent anticancer agents with unusual redox features. *Inorg. Chem.* **2018**, *57*, 1705−1716.
(27) Du, Q.; Yang, Y.; Guo, L.; Tian, M.; Ge, X.; Tian, Z.; Zhao, L.; Xu, Z.; Li, J.; Liu, Z. Fluorescent half-sandwich phosphine-sulfonate iridium(III) and ruthenium(II) complexes as potential lysosome-targeted anticancer agents. *Dyes Pigm.* **2019**, *162*, 821−830.
(28) Du, Q.; Guo, L.; Tian, M.; Ge, X.; Yang, Y.; Jian, X.; Xu, Z.; Tian, Z.; Liu, Z. Potent half-sandwich iridium(III) and ruthenium(II) anticancer complexes containing a P^O-chelated ligand. *Organometallics* **2018**, *37*, 2880−2889.
(29) Zhao, J.; Li, W.; Gou, S.; Li, S.; Lin, S.; Wei, Q.; Xu, G. Hypoxia-targeting organometallic Ru(II)−arene complexes with enhanced anticancer activity in hypoxic cancer cells. *Inorg. Chem.* **2018**, *57*, 8396−8403.
(30) Liu, Z.; Romero-Canelón, I.; Qamar, B.; Hearn, J. M.; Habtemariam, A.; Barry, N. P. E.; Pizarro, A. M.; Clarkson, G. J.; Sadler, P. J. The potent oxidant anticancer activity of organoiridium catalysts. *Angew. Chem., Int. Ed.* **2014**, *53*, 3941−3946.
(31) Movassaghi, S.; Singh, S.; Mansur, A.; Tong, K. K. H.; Hanif, M.; Holtkamp, H. U.; Söhnel, T.; Jamieson, S. M. F.; Hartinger, C. G. (Pyridin-2-yl)-NHC organoruthenium complexes: antiproliferative properties and reactivity toward biomolecules. *Organometallics* **2018**, *37*, 1575−1584.
(32) Jeyalakshmi, K.; Haribabu, J.; Balachandran, C.; Swaminathan, S.; Bhuvanesh, N. S. P.; Karvembu, R. Coordination Behavior of N,N′,N″-trisubstituted guanidine ligands in their Ru-arene complexes: Synthetic, DNA/protein binding, and cytotoxic studies. *Organometallics* **2019**, *38*, 753−770.
(33) Yang, Y.; Guo, L.; Tian, Z.; Gong, Y.; Zheng, H.; Zhang, S.; Xu, Z.; Ge, X.; Liu, Z. Novel and versatile imine-N-heterocyclic carbene half-sandwich iridium(III) complexes as lysosome-targeted anticancer agents. *Inorg. Chem.* **2018**, *57*, 11087−11098.
(34) Zamora, A.; Pérez, S. A.; Rothemund, M.; Rodríguez, V.; Schobert, R.; Janiak, C.; Ruiz, J. Exploring the influence of the

DOI: 10.1021/acs.organomet.9b00080
Organometallics XXXX, XXX, XXX−XXX

aromaticity on the anticancer and antivascular activities of organoplatinum(II) complexes. *Chem.—Eur. J.* **2017**, *23*, 5614−5625.
(35) Wenzel, M.; de Almeida, A.; Bigaeva, E.; Kavanagh, P.; Picquet, M.; Le Gendre, P.; Bodio, E.; Casini, A. New Luminescent Polynuclear Metal Complexes with Anticancer Properties: Toward Structure-Activity Relationships. *Inorg. Chem.* **2016**, *55*, 2544−2557.
(36) Yang, Y.; Guo, L.; Tian, Z.; Liu, X.; Gong, Y.; Zheng, H.; Ge, X.; Liu, Z. Imine-N-heterocyclic carbene as versatile ligands in ruthenium-(II) p-cymene anticancer complexes: A structure-activity relationship study. *Chem.—Asian J.* **2018**, *13*, 2923−2933.
(37) Kong, D.; Guo, L.; Tian, M.; Zhang, S.; Tian, Z.; Yang, H.; Tian, Y.; Liu, Z. Lysosome-targeted potent half-sandwich iridium(III) α-diimine antitumor complexes. *Appl. Organomet. Chem.* **2019**, *33*, No. e4633.
(38) Yang, Y.; Guo, L.; Ge, X.; Shi, S.; Gong, Y.; Xu, Z.; Zheng, X.; Liu, Z. Structure-activity relationships for highly potent half-sandwich organoiridium(III) anticancer complexes with C^N-chelated ligands. *J. Inorg. Biochem.* **2019**, *191*, 1−7.
(39) Rubbiani, R.; Kitanovic, I.; Alborzinia, H.; Can, S.; Kitanovic, A.; Onambele, L. A.; Stefanopoulou, M.; Geldmacher, Y.; Sheldrick, W. S.; Wolber, G.; Prokop, A.; Wölfl, S.; Ott, I. Benzimidazol-2-ylidene gold(I) complexes are thioredoxin reductase inhibitors with multiple antitumor properties. *J. Med. Chem.* **2010**, *53*, 8608−8618.
(40) Daum, S.; Reshetnikov, M. S. V.; Sisa, M.; Dumych, T.; Lootsik, M. D.; Bilyy, R.; Bila, E.; Janko, C.; Alexiou, C.; Herrmann, M.; Sellner, L.; Mokhir, A. Lysosome-targeting amplifiers of reactive oxygen species as anticancer prodrugs. *Angew. Chem., Int. Ed.* **2017**, *56*, 15545−15549.
(41) Wang, H.; Joseph, J. A. Quantifying cellular oxidative stress by dichlorofluorescein assay using microplate reader11Mention of a trade name, proprietary product, or specific equipment does not constitute a guarantee by the United States Department of Agriculture and does not imply its approval to the exclusion of other products that may be suitable. *Free Radical Biol. Med.* **1999**, *27*, 612−616.
(42) Vellaisamy, K.; Li, G.; Ko, C.-N.; Zhong, H.-J.; Fatima, S.; Kwan, H.-Y.; Wong, C.-Y.; Kwong, W.-J.; Tan, W.; Leung, C.-H.; Ma, D.-L. Cell imaging of dopamine receptor using agonist labeling iridium(III) complex. *Chem. Sci.* **2018**, *9*, 1119−1125.
(43) Ma, X.; Jia, J.; Cao, R.; Wang, X.; Fei, H. Histidine−iridium(III) coordination-based peptide luminogenic cyclization and cyclo-RGD peptides for cancer-cell targeting. *J. Am. Chem. Soc.* **2014**, *136*, 17734−17737.
(44) Luzio, J. P.; Pryor, P. R.; Bright, N. A. Lysosomes: fusion and function. *Nat. Rev. Mol. Cell Biol.* **2007**, *8*, 622−632.
(45) Saftig, P.; Klumperman, J. Lysosome biogenesis and lysosomal membrane proteins: trafficking meets function. *Nat. Rev. Mol. Cell Biol.* **2009**, *10*, 623−635.
(46) He, L.; Tan, C.-P.; Ye, R.-R.; Zhao, Y.-Z.; Liu, Y.-H.; Zhao, Q.; Ji, L.-N.; Mao, Z.-W. Theranostic iridium(III) complexes as one- and two-photon phosphorescent trackers to monitor autophagic lysosomes. *Angew. Chem., Int. Ed.* **2014**, *53*, 12137−12141.
(47) Boya, P.; Kroemer, G. Lysosomal membrane permeabilization in cell death. *Oncogene* **2008**, *27*, 6434−6451.
(48) He, L.; Li, Y.; Tan, C.-P.; Ye, R.-R.; Chen, M.-H.; Cao, J.-J.; Ji, L.-N.; Mao, Z.-W. Cyclometalated iridium(III) complexes as lysosome-targeted photodynamic anticancer and real-time tracking agents. *Chem. Sci.* **2015**, *6*, 5409−5418.
(49) Li, J.; Tian, Z.; Xu, Z.; Zhang, S.; Feng, Y.; Zhang, L.; Liu, Z. Highly potent half-sandwich iridium and ruthenium complexes as lysosome-targeted imaging and anticancer agents. *Dalton Trans.* **2018**, *47*, 15772−15782.
(50) Wang, C.; Liu, J.; Tian, Z.; Tian, M.; Tian, L.; Zhao, W.; Liu, Z. Half-sandwich iridium N-heterocyclic carbene anticancer complexes. *Dalton Trans.* **2017**, *46*, 6870−6883.
(51) Crochet, P.; Gimeno, J.; Borge, J.; García-Granda, S. Novel ruthenium(II) complexes containing imino- or aminophosphine ligands for catalytic transfer hydrogenation. *New J. Chem.* **2003**, *27*, 414−420.
(52) Shirakawa, E.; Yoshida, H.; Takaya, H. An iminophosphine-palladium catalyst for cross-coupling of aryl halides with organostannanes. *Tetrahedron Lett.* **1997**, *38*, 3759−3762.
(53) Crossetti, G. L.; Filgueiras, C. A. L.; Howie, R. A.; Wardell, J. L.; Ziglio, C. M. Dibromo {N-[2-(diphenylphosphino)-benzylidene]-2,6-diisopropylaniline-k^2*N,P*} nickel. *Acta Crystallogr., Sect. C: Cryst. Struct. Commun.* **2001**, *57*, 1279−1281.
(54) Yoshida, H.; Shirakawa, E.; Kurahashi, T.; Nakao, Y.; Hiyama, T. Palladium−Iminophosphine-Catalyzed Alkynylstannylation of Alkynes. *Organometallics* **2000**, *19*, 5671−5678.
(55) Vaughan, T. F.; Koedyk, D. J.; Spencer, J. L. Comparison of the Reactivity of platinum(II) and platinum(0) complexes with iminophosphine and phosphinocarbonyl ligands. *Organometallics* **2011**, *30*, 5170−5180.
(56) Mogorosi, M. M.; Mahamo, T.; Moss, J. R.; Mapolie, S. F.; Slootweg, J. C.; Lammertsma, K.; Smith, G. S. Neutral palladium(II) complexes with P,N Schiff-base ligands: Synthesis, characterization and catalytic oligomerisation of ethylene. *J. Organomet. Chem.* **2011**, *696*, 3585−3592.
(57) Zheng, Q.; Zheng, D.; Han, B.; Liu, S.; Li, Z. Chromium complexes supported by the bidentate PN ligands: synthesis, characterization and application for ethylene polymerization. *Dalton Trans.* **2018**, *47*, 13459−13465.

DOI: 10.1021/acs.organomet.9b00080
Organometallics XXXX, XXX, XXX−XXX